CryoEM structures of the multimeric secreted NS1, a major factor for dengue hemorrhagic fever

Authors: Bo Shu, Justin S.G. Ooi, Aaron W.K Tan, Thiam-Seng Ng, Wanwisa Dejnirattisai, Juthathip Mongkolsapaya, Guntur Fibriansah, Jian Shi, Victor A. Kostyuchenko, Gavin Screaton, Shee-Mei Lok*

*Correspondence: Shee-Mei Lok (sheemei.lok@duke-nus.edu.sg)

Abstract

Dengue virus infection can cause dengue hemorrhagic fever (DHF). Dengue NS1 is multifunctional: the intracellular dimeric NS1 (iNS1) forms part of the viral replication complex, the extracellular multi-oligomeric secreted NS1 (sNS1) is a major factor contributing to DHF. The structure of the iNS1 is well studied but not sNS1. Here we show the tetrameric (stable and loose conformation) and hexameric structures of sNS1. Stability of the stable and loose tetramers is determined by the conformation of their N-terminal domain – elongated β-sheet or β-roll. Binding of an anti-NS1 Fab breaks the loose tetrameric and hexameric sNS1 into dimers, whereas the stable tetramer remains largely unbound. Our results show detailed quaternary organization of different oligomeric states of sNS1 and will contribute towards the design of dengue therapeutics.

Main

14 Dengue is a positive sense single-stranded RNA enveloped virus. It belongs to the
15 family *Flaviviridae*, which also includes significant human pathogens like West Nile (WNV),
16 yellow fever (YF) and Zika virus (ZIKV). Dengue virus causes disease that ranges from mild
17 dengue fever to the severe dengue hemorrhagic fever (DHF) and the dengue shock syndrome
18 (DSS)[1]. There are four DENV serotypes. Dengvaxia, which is currently the only licensed
19 dengue vaccine, has an overall efficacy of only 45%, and there is a possibility of priming the
20 previously immune naïve children to develop severe disease in subsequent natural infection
21 after vaccination [2]. It has proven to be difficult to develop an effective vaccine using whole
22 dengue virus or its surface E protein, as the vaccine would need to stimulate equally strong
23 immune responses simultaneously against all four dengue serotypes or else it can lead to a
24 possibility of antibody-dependent enhancement (ADE) of infection[3]. This could lead to severe
25 DHF/DSS.

26 Recently, dengue non-structural protein 1 (NS1) has been investigated as an alternative
27 protein candidate for vaccine development. It has been shown to play an important role in
28 causing the vascular leakage symptoms in DHF/DSS[4]. NS1 is secreted alongside dengue virus
29 particles during an infection. It is a multifunctional protein which exists in different oligomeric
30 forms intracellularly and extracellularly[5], and they play distinctly different roles. The
31 intracellular NS1 (iNS1), exists as membrane associated dimeric form and is a part of the viral
32 replication complex. The extracellular secreted NS1 (sNS1), exists in higher oligomeric forms.
33 sNS1 likely causes vascular leakage symptoms in DHF/DSS via two pathways – indirectly, by
34 stimulating the innate immune response through activation of complement and Toll-like
35 receptors[6], and directly, by binding to endothelial cells causing endothelial hyperpermeability.
36 sNS1 when bound directly to endothelial cells causes barrier dysfunction of the cell monolayer
37 as demonstrated in an *in vitro* trans-endothelial electrical resistance (TEER) assay[4,7]. *In vivo*

38 studies show that the sNS1 is present at very high concentrations in patient sera and correlates
39 closely with the severity of disease [8]. Mice injected with sNS1 along with a sublethal dose of
40 DENV were observed to succumb to infection. Injection of sNS1 alone also causes vascular
41 leakage in mice[4]. NS1-immune polyclonal serum and anti-NS1 monoclonal antibodies (MAbs)
42 can protect mice against lethal DENV2 challenge [4]. sNS1 was also found to enhance viral
43 infection in mosquitoes by downregulating mosquito midgut immune genes[9]. sNS1 is therefore
44 an important viral protein both for viral infection (mammalian cells and mosquitoes) and
45 pathogenesis, and it is important to understand the structure of the sNS1 protein.

46 iNS1 (45 kDa) is first made in the endoplasmic reticulum (ER) as a monomer. It then
47 forms dimers and is glycosylated in the ER and the trans-Golgi network. It is eventually
48 transported to the cell membrane where some is secreted outside the cell, becoming sNS1.
49 There is a high-resolution crystal structure of full length dimeric dengue iNS1[10] produced by
50 baculovirus expression and subsequent extraction from cellular membrane compartments .
51 There are also crystal structures of the dimeric form of NS1 protein from other flaviviruses[11]
52 and they are largely similar to that of the DENV iNS1. Each protomer of the iNS1 contains
53 three domains (Extended data Fig. 1A): 1) the N-terminus contains the β-roll domain (amino
54 acids 1-30) that interacts with the same domain from the other protomer within the dimer to
55 form a roll-like structure (named β-roll). This domain is generally hydrophobic and is thought
56 to interact with cellular membranes. 2) Following the β-roll domain is the wing domain (amino
57 acids 31-181). The wing domain is the most flexible domain as it differs between different
58 flavivirus NS1 crystal structures [11]. 3) the β-ladder domain (amino acids 182-352), consists of
59 a continuous arrangement of 10 β-strands. The β-ladder domains from the two iNS1 protomers
60 line up with each other to form a long ladder-like pattern. One side of the β-ladder faces the
61 hydrophobic β-roll, while the other side is decorated with its highly charged spaghetti loops.

62 The interaction between protomers within the dimer is stabilized by a large number of hydrogen
63 bonds[12].

64 About a decade ago, two very low resolution (23 Å and 30 Å) EM structures of sNS1
65 were determined: a cryoEM structure reconstructed from images acquired by using an 120kV
66 LaB_6-equipped electron microscope (Philip CM12 TEM)[13] and the other, a negative stained
67 room temperature EM structure (Extended data Fig. 1B)[14]. Both maps had an overall hollow
68 barrel-like structure lacking fine structural details. Since then, the availability of 300kV
69 transmission electron microscopes equipped with direct electron detectors and field emission
70 gun electron sources, as well as improved cryoEM reconstruction methods, have made more
71 routine determination of cryoEM structures of small proteins to high resolution possible. Here
72 we report the cryoEM structures of DENV2 sNS1 tetramers (dimer of dimers) and hexamers
73 (trimer of dimers). We observe sNS1 exists predominantly in the tetrameric form. There are
74 two tetrameric states - stable and loose, and some of these structures are determined to ~3.5Å
75 resolution. The most obvious and dramatic difference between the stable and loose tetramers
76 is the organization of their N-terminal domains – elongated β-sheet and β-roll, respectively.
77 Only a minority of the sNS1 population is hexameric and this cryoEM structure was determined
78 to 8Å resolution. We also determined a structure of sNS1 complexed with a Fab 5E3 to 3.5Å
79 resolution. Most of the sNS1 (loose tetramers and hexamers) dissociates into dimers when
80 bound to Fab, while the stable tetramer remains largely unbound. This is consistent with our
81 results showing the ability of the Fab 5E3 to only partially inhibit sNS1-induced endothelial
82 cell permeability. This study shows sNS1 exists in a heterogenous mixture of oligomerization
83 states, and we present the first high resolution structures of sNS1.

84

85 **sNS1 from DENV2 contains heterogenous oligomeric states with tetramers as the**
86 **predominant population.**

His-tagged NS1 was expressed in human embryonic kidney (HEK) cells. We harvested the sNS1 from tissue culture supernatant and after purification, we analyzed it using coomassie blue stained semi-denaturing SDS-PAGE gel (the sample was not boiled nor exposed to DTT). The gel shows clear bands corresponding to dimers and tetramers (Fig. 1A). As the sample was exposed to SDS, a detergent, the presence of tetramer band suggests that the tetramer is resistant to detergent. We then performed cross-linking of sNS1 with bis(sulfosuccinimidyl) suberate (BS^3) before analyzing it by denaturing SDS-PAGE. This showed the presence of aggregates, which could be due to BS^3 non-specifically crosslinking proteins, as well as bands for hexamer, tetramer, dimer and monomer (Fig. 1B). These results also showed that the tetrameric form is the predominant oligomerization state in the NS1 protein sample.

We collected 7714 cryoEM micrographs and observed particles with distinct shapes (Fig. 1C). We then performed several cycles of 2D classification and alignment of the boxed particles. The 2D class averages show particles with different features (Fig. 1D) - some appearing like stable and loose tetramers and others like hexamers. We did not observe any sNS1 dimers. This suggests that sNS1 consists of heterogenous populations of particles with likely tetrameric and hexameric states.

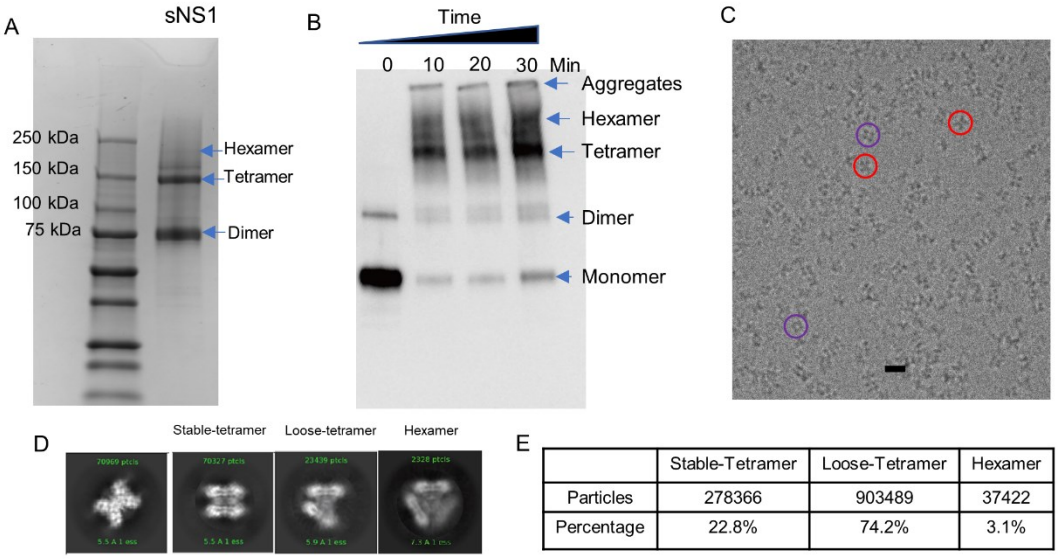

	Stable-Tetramer	Loose-Tetramer	Hexamer
Particles	278366	903489	37422
Percentage	22.8%	74.2%	3.1%

Fig. 1 Profile of the DENV2 sNS1. **(A)** Semi-denaturing SDS-PAGE gel (non-boiling and no DTT) shows the clear dimer and tetramer bands, along with a very faint hexamer band. **(B)** Western blot denaturing SDS-PAGE gel (using Anti-polyHistidine−Peroxidase antibody) analysis of sNS1 cross-linked with BS^3 at different incubation times. Aggregates, hexamers, tetramers, dimers and monomers were seen. (**C**) A cryoEM micrograph of the sNS1 showing distinct-shaped particles, e.g., butterfly-shaped (red circles) and cube-shaped particles (purple circles). Scale bar is 10 nm. (**D**) The 2D class averages indicate that the particles are heterogenous, with some likely existing as tetramers (stable and loose forms) and others as hexamers. (**E**) The distribution of particles in different oligomerization states determined after 3D classification and refinement. Most of the particles are tetramers (loose and stable) and hexamers are a minority in the population.

116 **CryoEM reconstruction of different oligomeric states of sNS1**

117 As sNS1 consists of a heterogenous population of particles of different oligomerization
118 states, we performed a 3D classification using the program Relion [15]. The first round of
119 unsupervised classification was done assuming no symmetry (C1) to avoid bias towards any
120 specific oligomerization states. We then performed rough fitting with a dimeric NS1 crystal
121 structure into these maps to determine their oligomerization states (Extended data Fig. 2). We
122 observed two maps that correspond to tetramers: one with clear densities suggesting that the
123 overall structure is quite stable (Extended data Figs. 2), while the other with looser interactions
124 between the two dimers and poorer map resolution. We refer the former as stable tetramer and
125 the latter, as loose tetramer. We also observed a 3D class that is hexameric in structure.
126 Consistent with the 2D class averages, the 3D classification also did not yield any dimeric
127 structures. We then conducted further classification and refinement. For the stable tetramers,
128 we imposed D2 symmetry and obtained a final map of 3.5Å resolution (Fig. 2A), as measured
129 by gold standard FSC curve cutoff at 0.143. For the loose tetramers, no symmetry was imposed,
130 and we determined one subclass of the loose tetramer to 8 Å resolution (Fig. 3A(i) and
131 Extended data Fig. 4A). We then performed local refinement on one of its dimers and obtained
132 a 3.4 Å cryoEM density map (Fig. 3A(ii) and Extended data Fig. 4B). For the hexamers, since
133 we only had a limited number of particles (~30,000 particles), we obtained an 8Å map (Figs.
134 3B and Extended data Fig. 5).

135 **Structure of sNS1 stable tetramers**

136 The 3.5Å resolution sNS1 stable tetramer cryoEM map shows clear separation between
137 β-strands (Extended data Figs. 3C-D). We also calculated the local resolution (Extended data
138 Fig. 3A) of the map. While most of the density map is ~3.5 Å resolution, parts of the map
139 (corresponding to the β-ladder) are at ~3.0Å resolution with some of the side chain densities
140 resolved (Extended data Fig. 3D). The resolution of the wing domain and the β-roll was lower

141 (4.0 to 4.5 Å). The density of both N- (residues 1-11) and C- terminal ends (residues 341-352)
142 is missing from the map.

143 We interpreted the stable tetramer (dimer of dimers) cryo-EM density by fitting in the
144 zika dimeric NS1 crystal structure (PDB:5GS6), because the structure is more complete than
145 the dengue iNS1, and then mutated it into dengue NS1 sequence (Figs. 2A-B and Extended
146 data Fig.3B). After fitting, we compared one of our sNS1 dimer in the stable tetramer to the
147 dengue iNS1 dimer (PDB:4O6B) and it shows the wing domain of our sNS1 dimer is rotated
148 by 6.8° with respect to the β-ladder. The β-roll structures of the two dengue iNS1 dimers cannot
149 fit well into the cryoEM density of the stable tetramer and they clash with each other. Indeed,
150 the space (25Å) between two dimers within the stable tetramers is not big enough to
151 accommodate the two iNS1 β-rolls. We observed that the β-roll densities, instead of
152 concentrating at the middle of the dimers as observed in iNS1 (Extended data Fig. 1), have an
153 elongated shape that stretches across the two protomers within a dimer (Figs. 2A and B). This
154 suggests that they have very different tertiary structures. Fitting of the density map shows that
155 residues 15 to 24 form a long β-strand which pairs with the same β-strand of the other protomer
156 within the dimer to form a long anti-parallel β-sheet (hereafter, referred to as elongated β-sheet)
157 (Figs 2A-B). As the resolution of this region is ~4.5 Å, we analyzed their interaction by using
158 a distance cut off of 8 Å between the Cα backbone. Using this criterion, we observed that this
159 elongated β-sheet from one dimer likely interacts with the same β-sheet from the opposite
160 dimer via electrostatic interactions or hydrogen bonds at both ends of each respective β-sheet
161 (Fig. 2C(i)-(ii)). Charge analysis in UCSF Chimera [18] shows that these two ends have high
162 charge complementarity between dimers (Fig. 2C (iii)), suggesting possible hydrogen bonds or
163 electrostatic interactions. Hydrophobic analysis shows that these β-sheets have an overall
164 highly hydrophobic surface that also plays an important role in stabilizing their interactions.

We next compared the β-roll domain of iNS1 with the elongated β-sheet of the sNS1 stable tetramer. The iNS1 β-roll domain contains three β-strands (residues 1-7, 12-16 and 18-22), whereas we were unable to observe any density for residues 1-11 in the sNS1 stable tetramer, probably due to disorder in this region, and residues 15-24 form a long, continuous β-strand. This raises a question: is the sNS1 tetramer assembled from dimers of iNS1? If so, is it possible for the iNS1 β-roll structure to rearrange into the elongated β-sheet seen in the stable tetramer? If this were to happen, it would require the second β-strand of iNS1 to rotate by ~120° with respect to the third β-strand to form the long, continuous β-strand we observed (Fig. 2D). Whether the iNS1 dimer is a precursor of the sNS1 stable tetramer is unknown. It is also possible that the sNS1 stable tetramer is assembled during translation of the NS1 protein by a pathway independent of iNS1 dimer formation, before being secreted.

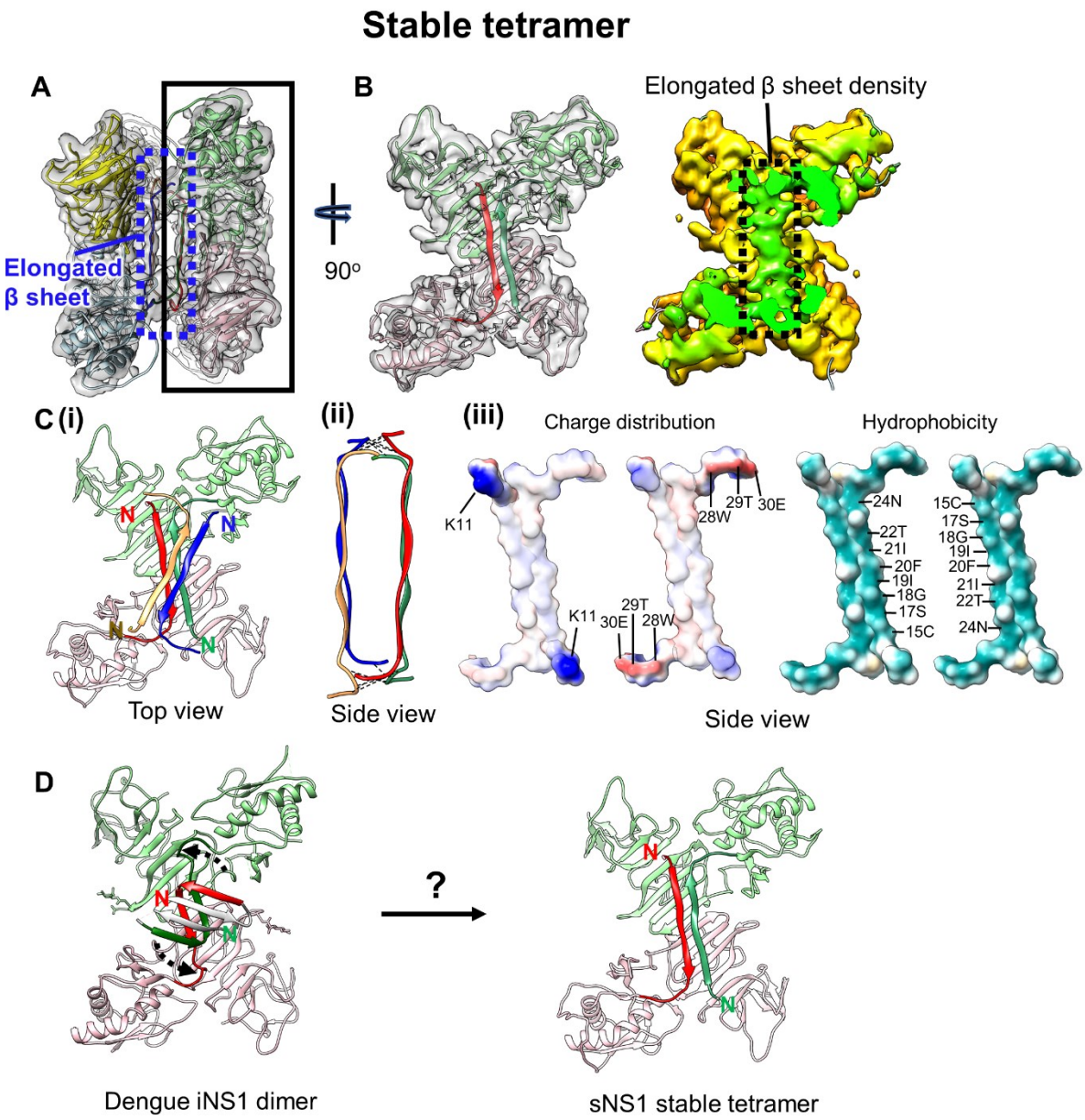

Fig. 2 Structure of the stable sNS1 tetramer. (**A**) Two NS1 dimeric structures fitted into the cryoEM map (reduced sharpening was applied to make the density of the elongated β-sheet clearer). One dimer is colored in pink and light green and the other in yellow and light blue. (**B**) Left: the overall structure of the sNS1 dimer is similar to that of iNS1 except for the β-roll region (residues 1-30) in iNS1, which is an elongated β-sheet (residues 15-24) in sNS1. View from the elongated β-sheet of the black boxed region in (A). The respective elongated β-strand of each protomer is highlighted in a darker shade of the same color (red and dark green). Right: surface density map with the regions corresponding to the elongated β-sheet colored in green, and the rest of the map in yellow. (**C**) Interaction of the elongated β-strands between the two dimers (red/green and yellow/blue). (i) Top view showing the elongated β-sheets of the red/green dimer interacting with that of the yellow/blue dimer (only its elongated β-sheet is shown). (ii) Side view showing possible hydrogen bonds or electrostatic interactions between the two elongated β-sheets from opposite dimers (dotted black lines). These interactions are

identified by the distance between Cα backbone (< 8Å) and also their charge characteristics. (iii) The interacting residues are complementary in both charges and hydrophobicity. Open book representation of (ii): (Left) charge, and (Right) hydrophobicity distributions on the surface of the two elongated β-sheets. For charge, positive charges are colored in blue while negative charges are red. For hydrophobicity, cyan color indicates hydrophobic residues. Possible interacting residues are labelled. **(D)** Comparison of iNS1 β-roll with sNS1 stable tetramer elongated β sheet and how it might change from the β-roll structure (dotted arrow on the iNS1 structure) into the elongated β sheet structure.

200

201 **CryoEM structure of loose sNS1 tetramers**

202 We also determined an 8Å resolution loose sNS1 tetramer structure (Figs. 3A(i) and
203 Extended data Fig.4A) and by focused refinement on one of its constituent dimers, we obtained
204 a 3.4Å resolution cryoEM map (Figs. 3A (ii) and Extended data Fig.4B (i-ii)). The overall
205 structure of the dimer and its β-roll (Fig. 3A (ii)) is very similar to that of iNS1 (RMSD 0.8 Å),
206 unlike the stable sNS1 tetramer. The overall 8Å resolution loose sNS1 tetramer structure shows
207 that the two dimers are rotated by ~35° with respect to each other and extra density is visible
208 between the β-rolls of these two dimers (Fig. 3A(i)). Our high resolution sNS1 dimer structure
209 within the loose tetramer also shows some strong extra densities above the β-roll (Fig. 3A(iii)).
210 Previous work from other research groups [13,14] show that there are lipids associated with sNS1
211 that may help stabilize the overall structure, and which may contribute to these uninterpreted
212 densities.

213 The difference between the stable and the loose tetramers is whether the residues near
214 the N-terminus form a β-roll or an elongated β-sheet. Hence, this could be the determinant that
215 defines stability.

216 An existing crystal structure of a ZIKV sNS1 [11] (PDB code: 5GS6), obtained by
217 purifying sNS1 produced using a baculovirus expression system, is a dimeric structure.
218 However, upon examination of the crystal packing in this structure, sNS1 appears to have a
219 tetrameric structure similar to our loose tetramer (RMSD 4.2 Å) (Fig. 3A(iv)). This may
220 suggest that at least one of the ZIKV sNS1 oligomers might be the loose tetramer structure.

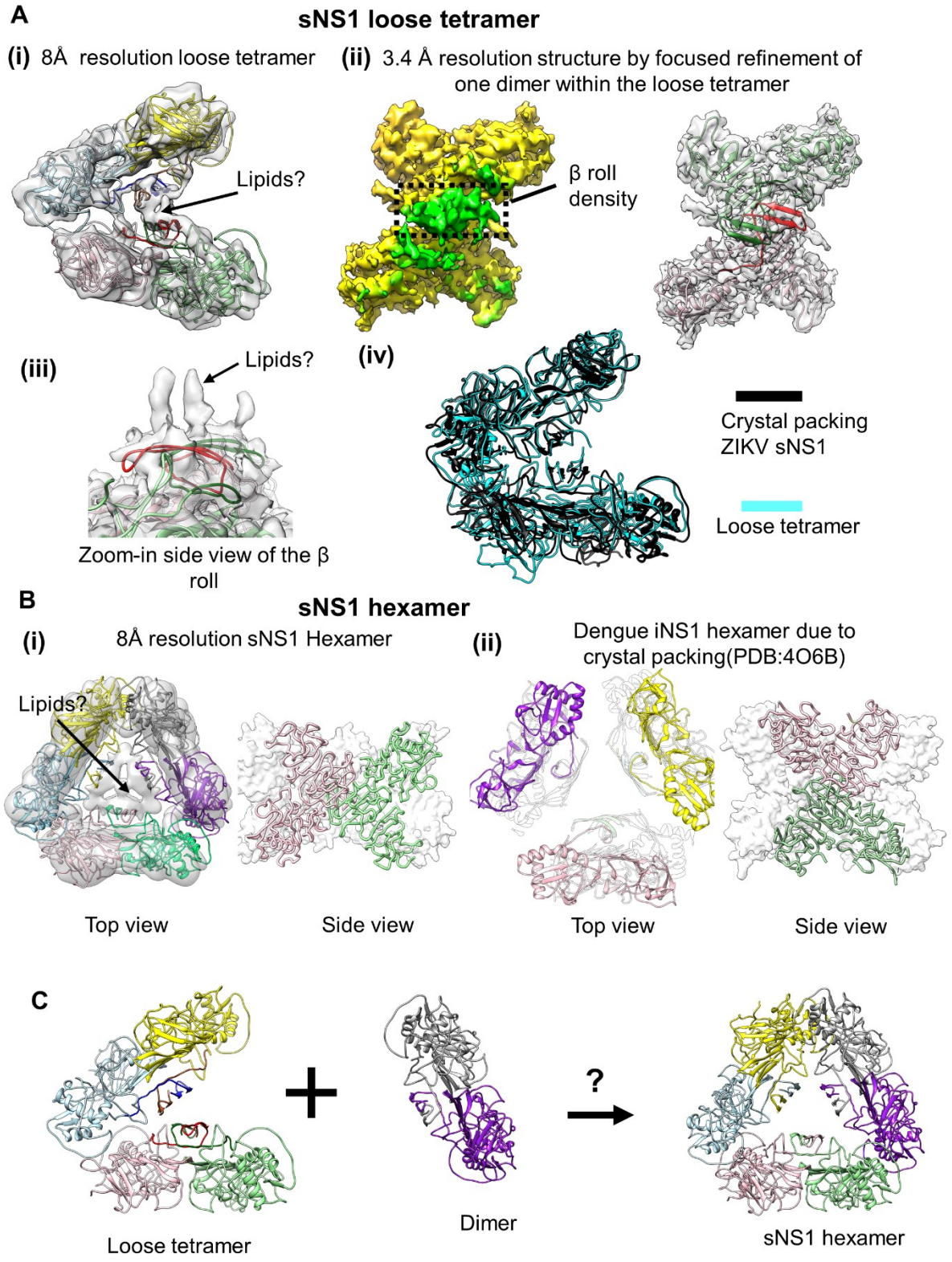

Fig. 3 CryoEM structures of the sNS1 loose tetramer and hexamer. **(A)** (i) The fit of sNS1 into the 8 Å resolution loose tetramer density map. (ii) Focused refinement of one dimer of the loose tetramer yields a 3.4Å resolution map. An iNS1 dimer fits well into the density showing that the loose tetramer contains a β-roll structure similar to that of iNS1. Left: cryoEM map with the density corresponding to the β-roll colored in green and the rest in yellow. Right: the fit of

the red/green dimer into the density. (iii) Zoom-in side view of the β-roll density (from (ii)) showing uninterpreted density that might belong to lipid molecules. (iv) Superposition of our loose tetramer with the tetramer observed in the crystal packing of ZIKV sNS1 structure (PDB: 5GS6) shows that they have similar structures. **(B)** Comparison of our sNS1 hexamer with the dengue iNS1 hexamer from the crystal packing. (i) Top and side views of the 8Å resolution sNS1 hexamer structure. Left: fit of three dimers into the cryoEM map. We are unable to discern whether sNS1 adopts a β-roll or an elongated β-sheet structure, as the interior of the hexamer contains unfeatured density. It may also contain lipid cargo as suggested by Gutsche and colleagues [14] (ii) The previously published dengue iNS1 structure [10] shows hexamers due to crystal packing; however, there is little interaction between the iNS1 dimers (left; top view). The dimers in the hexamer (right; side view) are also oriented differently to our hexameric structure (in (i), side view). **(C)** Interaction of a loose tetramer with a dimer could lead to the formation of a hexamer.

241 **CryoEM structure of the sNS1 hexamer**

242 We obtained an 8Å resolution sNS1 hexamer map (Figs. 3B(i) and Extended data Fig.
243 5A-B). The low resolution structure suggests that the NS1 molecules in the hexameric state are
244 interacting loosely with each other. Fitting of iNS1 (Extended data Fig. 5C) suggests that three
245 dimers interact with each other via their wing domain and the distal end of the β-ladder. This
246 interaction is similar to that in the loose tetramer. The density in the central core of the hexamer
247 is weak (Extended data Fig. 5B) and we were therefore unable to determine if the dimers have
248 a β-roll or elongated β-sheet conformation. It is also possible that the interior of this hexamer
249 contains lipid cargo, as suggested by other research groups [13,14] and this may prevent
250 determination of the structure of this region.

251 The crystal structure of dengue dimeric iNS1 [10] shows that the crystal packing contains
252 a trimer of dimers (i.e., hexamer) organization; however, there are very few interactions
253 between the three dimers (Fig. 3B(ii)). Their positions in the crystal lattice are mainly
254 supported by their interactions with other iNS1 molecules inside the crystal unit cell. This
255 suggests that the hexameric packing of iNS1 may not be physiological. Comparison of our
256 cryoEM sNS1 hexamer to this crystal hexamer packing shows a very different organization of
257 dimers –they are rotated by ~90° relative to each other (Fig. 3B(i) and (ii), right).

258 It is possible that the loose tetrameric structure is a transition intermediate of the
259 hexameric structure (Fig. 3C). However, we observed loose tetramers forming ~74% of the
260 particle population (Fig. 1D), while hexamers only form ~3%, suggesting that the loose
261 tetramer may be a preferred or a lower energy oligomerization state.

262 It is possible that both the loose tetrameric and the hexameric structures are stabilized
263 by lipids. To test this, we incubated the NS1 sample with detergent (0.05% DDM) and imaged
264 it by cryoEM SPA. We observed that the percentage of loose tetramers and hexamers decreased
265 dramatically after detergent treatment (Extended data Table 1), compared to untreated NS1

266 (Fig. 1E). This suggests that the lipids inside the loose tetramers and hexamers could be
267 important for their structural integrity. A caveat to this conclusion is the detergent could also
268 disrupt the hydrophobic interactions between the dimers.

269 **CryoEM structure of sNS1 complexed with Fab 5E3**

270 We also investigated the cryoEM structure of sNS1 complexed with the Fab fragment
271 of an anti-NS1 antibody 5E3. The 2D class averages (Fig. 4A) of the boxed particles from the
272 cryoEM micrographs suggest that, when bound by Fabs, most sNS1 particles become dimeric.
273 Unbound stable tetramers were also present (Fig. 4A) and formed ~18% of the total particles.
274 It suggests that the Fab 5E3 can readily dissociate the sNS1 loose tetrameric and hexameric
275 structures. The stable tetrameric structure, on the other hand, is more resistant to Fab binding.

276 The structure of the Fab 5E3:sNS1 dimer complex was determined to an overall
277 resolution of 3.5Å (Fig. 4B, and Extended data Fig. 6A), as measured by gold standard FSC
278 curve cutoff at 0.143 (Extended data Fig. 6B). The sNS1 dimer:Fab complex has an overall
279 arch shape, where the Fabs bind to both ends of the β-ladders of the sNS1 dimer (Fig. 4B and
280 Extended data Fig.6A) and are tilted towards the β-roll side of the sNS1.

281 Fab 5E3 interacts with the end of the β-ladder of NS1 (Fig. 4B, Extended data Figs. 6-
282 7) via mainly the Fab heavy chain (Extended data Table 2). The 5E3 epitope is similar to two
283 other previously published Fab:NS1 dimer complex [19,20] – Fabs 2B7 and 1G5.3 (Extended data
284 Fig. 7). Comparison of these structures shows that these three Fabs bind at different angles to
285 the NS1 β-ladder. It has been postulated previously[10] that the hydrophobic β-roll may bind
286 directly to cellular membranes (Extended data Fig. 1), which could be important for its
287 pathogenesis, and therefore the binding orientation of Fab 5E3 may hinder this interaction. A
288 similar neutralization mechanism was suggested for Fab 2B7 [20].

289 We observed that these NS1 dimers have β-roll structures (Figs. 4B and Extended data
290 Fig.6C). This suggests that they are likely not derived from the stable tetramer which has an
291 elongated β-sheet structure. Hence, they could be a broken down product of Fab binding to
292 sNS1 loose tetramers (which contain β-roll structures) and perhaps also the hexamers. We
293 superimposed the Fab:dimer complexes into the loose tetramer and hexamer, and they showed
294 Fabs when bound, could clash with the neighbouring NS1 dimer (Extended data Fig. 8A-B).
295 Analysis of the solvent accessibility of the epitopes on the loose tetramer (Extended data Fig.
296 8C) shows two of the epitopes (orange spheres) are partially exposed (37.5%), while the other
297 two (cyan spheres), are fully exposed. All epitopes in the hexamer (Extended data Fig. 8D) are
298 partially exposed (37.5%). Since Fab likely could bind to the loose tetramer and hexamer. This
299 suggests that the loose tetramers and hexamers likely undergo motions that will at some time
300 point, have their epitopes fully exposed for Fab binding, and once the Fab has bound, the loose
301 tetramer and hexamers could be dismantled into dimers.

302 We reconstructed the unbound stable tetramer to 3.9Å resolution (Fig. 4C (i)), it is
303 identical to the uncomplexed stable tetramer (Fig. 2). Analysis of the epitopes on all NS1
304 molecules in the unbound stable tetramer shows they are only partially exposed (37.5%)
305 (Extended data Fig. 8E), thus discouraging Fab binding. Superposition of the Fab 5E3:dimer
306 complex with one of the dimers in the stable tetramer structure (Fig. 4C (ii)) also shows that
307 the Fab if bound, will clash with the wing domain of the neighbouring dimer. While the Fab is
308 able to cause dissociation between dimers in the loose tetramer and hexamer, it is unable to do
309 the same to the stable tetramer. This suggests that the two dimers in the stable tetramer have
310 tighter interactions, thus disallowing antibody binding. The presence of unbound stable
311 tetramer is consistent with the results of the TEER assay (Fig. 4D), showing Fab can only
312 partially inhibit sNS1 induced endothelial cell hyperpermeability.

313 In conclusion, since the loose tetramer and hexamers are less stable, their quaternary
314 structure can be easily disrupted by antibody binding. This may form part of the antibody
315 neutralization mechanism. The stable tetramer is however more resistant to Fab 5E3 binding,
316 and this may help sNS1 to evade the host immune response.

317

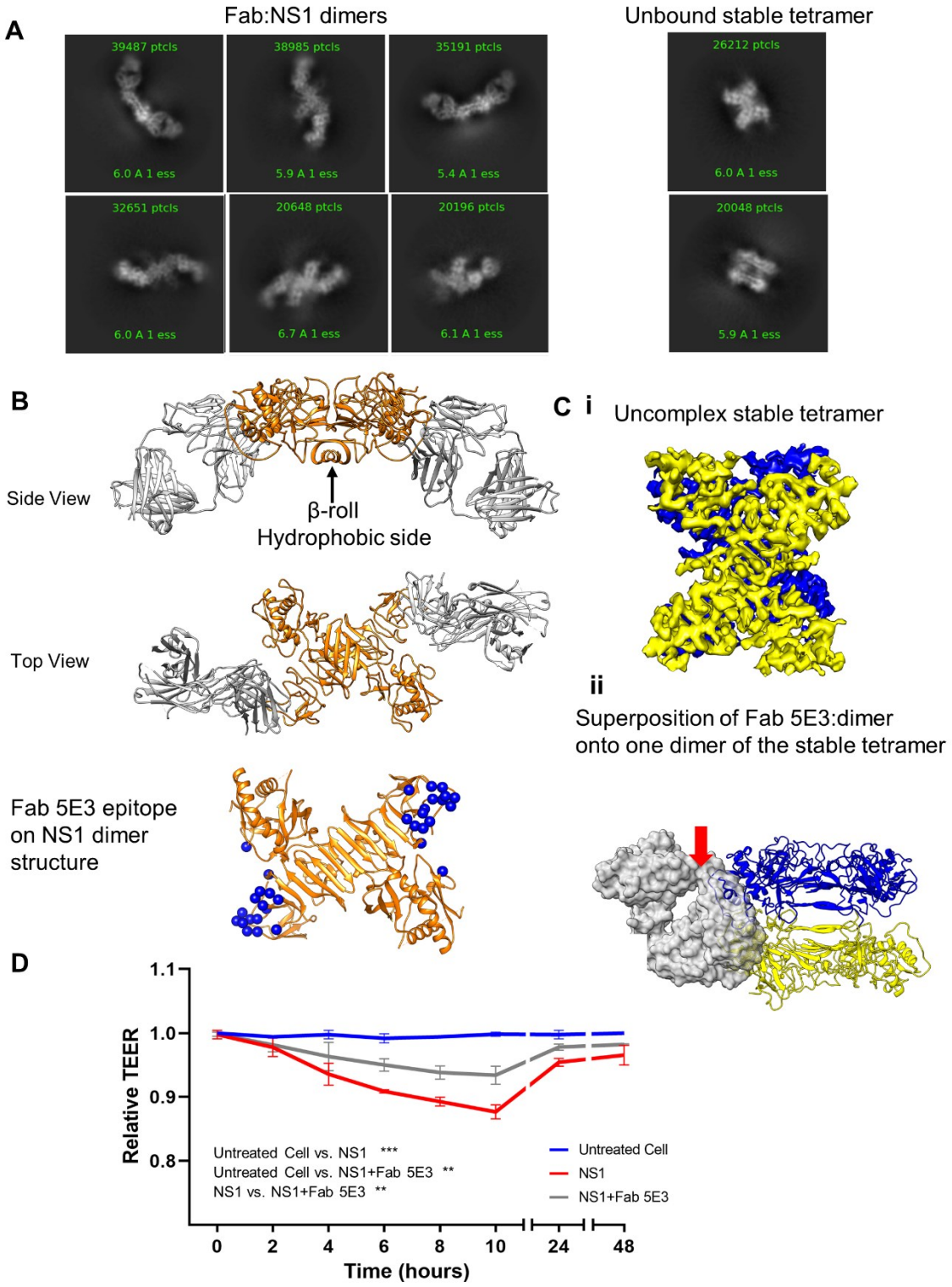

Fig. 4 CryoEM structure of sNS1 complexed with Fab 5E3. **(A)** Some of the 2D class averages showing Fab bound dimers and also unbound stable tetramers. **(B)** The 3.5Å resolution structure of dimer NS1(orange) complexed with Fab 5E3 (grey) shows that they form an arch shape – the Fabs are bending towards the β-roll side of the sNS1 dimer. This NS1 dimer contains the β-roll structure which is also present in the loose tetramer and the hexamer. The

Fabs bind to the ends of the β-ladder. The 5E3 epitope is shown as blue spheres. **(C) (i)** The 3.9Å resolution sNS1 unbound tetramer map. The two dimers of the tetramer are colored in blue and yellow. **(ii)** Superposition of Fab 5E3:dimer onto one dimer (yellow) of the stable tetramer shows that Fab (transparent grey surface) when bound will clash (red arrow) with the neighboring dimer (blue). **(D)** TEER assay showing Fab 5E3 can only partially prevent sNS1 from inducing human umbilical vein endothelial cell hyperpermeability. Data are the mean ± SEM from three independent experiments. Statistically significant differences between distinct groups (all time points combined for each group) compared to the untreated groups were determined by a two-way ANOVA analysis using Dunnett's test for multiple comparisons. (***$p < 0.001$ and **$p < 0.01$).

335 ## Discussion

336 Previous studies [13,14,21] and our cross-linking experiments of sNS1 (Fig. 1B)
337 consistently showed the presence of dimers, tetramers, and hexamers in semi- and fully
338 denaturing SDS PAGE gel. Syzdykova *et al*. also showed by native gel that yellow fever virus
339 sNS1 consists of mainly tetramers with little hexamers [22]. Our cryoEM study shows the vast
340 majority of DENV2 sNS1 particles exist as tetramers, while the hexamer only forms a minor
341 population (Fig. 1E). Flamand and colleagues [21] performed small angle X-ray scattering (SAXS)
342 experiments on sNS1 and observed particles with a homogenous gyration radius of 10nm (100
343 Å), which they concluded were likely hexamers. When we measured the dimensions of our
344 cryoEM sNS1 tetrameric and hexameric structures (Extended data Fig. 2), their longest
345 dimensions are the same (~100 Å), thus correlating well with size of particles detected by the
346 SAXS[21]. This suggests that SAXS may not be able to effectively differentiate between the
347 heterogenous populations of the particles within the sNS1 sample.

348 NS1 plays multiple roles in dengue virus infection of mammalian cells and also
349 mosquitoes. It was shown that sNS1 is one of the major factors contributing to the development
350 of DHF/DSS in patients. Our cryoEM studies show structural details of this important sNS1
351 protein – (1) the quaternary organization of the different native oligomerization states, (2) how
352 an antibody could bind and dismantle the loose tetrameric and hexameric sNS1 structures and
353 also (3) how sNS1 stable tetramers could resist this antibody-induced disassembly. These
354 findings will contribute to the design of therapeutics and vaccines against severe dengue
355 disease.

356

357

358 **Methods**

359 **sNS1 cloning, expression and purification**

360 DENV 2 NS1-HisTag was cloned and expressed in Expi293 HEK cells. The sNS1 protein was
361 purified by using a HisTrap column (GE Healthcare) and a gel-filtration chromatography.
362 Protein purity was then assessed by SDS-PAGE.

363

364 **BS^3 cross-linking of protein**

365 BS^3, a cross-linker, were added to NS1 in PBS to a final concentration of 5mM and the samples
366 were incubated for 10, 20, 30 mins at room temperature. Reactions were stopped by adding
367 Tris·HCl, pH 7.5 to a final concentration of 50mM and then the sample was added the SDS-
368 PAGE loading buffer, boiled for 2 min and then analyzed on a 4–20 % SDS-PAGE gradient
369 gels (Bio-Rad). The protein bands were then transferred to a nitrocellulose membrane, probed
370 with anti-polyHistidine−peroxidase antibody and visualized by chemiluminescence.

371

372 **CryoEM sample preparation, image acquisition and reconstruction procedure**

373 sNS1 was plunged frozen in liquid ethane by using the Vitrobot Mark IV plunger (FEI,
374 Netherlands).

375 CryoEM micrographs of sNS1/ sNS1 complex were collected using a Titan Krios transmission
376 electron microscope. Images were recorded by movie mode, and the frames from each movie
377 were aligned using MotionCor2 [23] to produce full dose images. The astigmatic CTF parameters
378 were estimated and accounted for during orientation search. A total of 2,342,754 particles were
379 picked. 2D class averages of particles were done. We then performed 3D classification and
380 reconstruction using C1 symmetry using the program Relion [15] to remove broken and distorted
381 particles. For the class with stable tetramers, we performed classification and refinement by
382 imposing D2 symmetry. For the loose tetramers, we reconstructed the whole particle using C1
383 symmetry and also performed local refinement on one of its dimers. For the hexamers, we
384 imposed D3 symmetry. Resolution was determined by using gold standard Fourier shell
385 correlation and local map resolution was estimated with ResMap [25].

386

387 **Protein structure building**

388 The sNS1 structures were first interpreted by approximate fitting of the NS1 dimeric crystal
389 structure using "fit-in-map" function in Chimera [18]. We then fit individual residues into
390 densities [26]. We then refined the structures using the "phenix.real_space_refine" procedure in
391 the Phenix software package, with default parameters and rigid body refinement using
392 secondary-structure and torsion angle restraints [27]. The final coordinates containing an
393 asymmetric unit (i.e., a protomer in the stable tetramer structure) were then used to build the
394 biological unit (full tetramer) by using the command "sym" in UCSF Chimera [18]. The final
395 coordinates of the asymmetric units were checked using MolProbity [28]. Maps and structures
396 shown in the Figs were generated by using UCSF Chimera and Coot.

397

398 **TEER assay**

399 A monolayer of Human Umbilical Vein endothelial cells (80%–90% confluency) cultured in
400 T75 flasks were detached using trypsin-EDTA (0.25%). The cells were then resuspended using
401 fresh culture media and then counted using an automated cell counter. 60,000 cells (300 µL per
402 well) were seeded onto the apical side of Transwell inserts. Each Transwell was transferred
403 inside a 24-well format plate containing 1.5 mL of endothelial cell culture media. Transwells
404 containing endothelial cells were incubated at 37°C and 5% CO2 for 3~4 days, and 50% of the
405 culture medium was changed in each well 48 hours post-seeding. Cells were grown until the
406 TEER values reached ~ 160 to 170 Ohms (Ω), indicating 100% cell confluency. After this, 3
407 µg NS1 protein / NS1_Fab5E3 complex (molar ratio 1:1.2) was added to the apical side of the
408 Transwell insert. Electrical resistance values, measured in Ohms (Ω), were recorded at every
409 2-hour time-points following the addition of the proteins using an Epithelial Volt Ohm Meter
410 with the "chopstick" electrodes. Endothelial permeability was expressed as relative TEER
411 which represents a ratio of resistance values (Ω) as follows: (Ω experimental condition - Ω
412 medium alone)/(Ω nontreated endothelial cells - Ω medium alone).

413

414

415 **References**

416 1 Gubler, D. J. Dengue and dengue hemorrhagic fever. *Clin Microbiol Rev* **11**, 480-496,
417 doi:10.1128/CMR.11.3.480 (1998).
418 2 Thomas, S. J. & Yoon, I. K. A review of Dengvaxia(R): development to deployment. *Hum*
419 *Vaccin Immunother* **15**, 2295-2314, doi:10.1080/21645515.2019.1658503 (2019).
420 3 Halstead, S. B. Neutralization and antibody-dependent enhancement of dengue viruses. *Adv*
421 *Virus Res* **60**, 421-467, doi:10.1016/s0065-3527(03)60011-4 (2003).
422 4 Beatty, P. R. *et al.* Dengue virus NS1 triggers endothelial permeability and vascular leak that
423 is prevented by NS1 vaccination. *Sci Transl Med* **7**, 304ra141,
424 doi:10.1126/scitranslmed.aaa3787 (2015).
425 5 Carpio, K. L. & Barrett, A. D. T. Flavivirus NS1 and Its Potential in Vaccine Development.
426 *Vaccines (Basel)* **9**, doi:10.3390/vaccines9060622 (2021).
427 6 Modhiran, N. *et al.* Dengue virus NS1 protein activates immune cells via TLR4 but not TLR2
428 or TLR6. *Immunol Cell Biol* **95**, 491-495, doi:10.1038/icb.2017.5 (2017).
429 7 Puerta-Guardo, H., Glasner, D. R. & Harris, E. Dengue Virus NS1 Disrupts the Endothelial
430 Glycocalyx, Leading to Hyperpermeability. *PLoS Pathog* **12**, e1005738,
431 doi:10.1371/journal.ppat.1005738 (2016).
432 8 Libraty, D. H. *et al.* High circulating levels of the dengue virus nonstructural protein NS1 early
433 in dengue illness correlate with the development of dengue hemorrhagic fever. *J Infect Dis*
434 **186**, 1165-1168, doi:10.1086/343813 (2002).
435 9 Liu, J. *et al.* Flavivirus NS1 protein in infected host sera enhances viral acquisition by
436 mosquitoes. *Nat Microbiol* **1**, 16087, doi:10.1038/nmicrobiol.2016.87 (2016).
437 10 Akey, D. L. *et al.* Flavivirus NS1 structures reveal surfaces for associations with membranes
438 and the immune system. *Science* **343**, 881-885, doi:10.1126/science.1247749 (2014).
439 11 Xu, X. *et al.* Contribution of intertwined loop to membrane association revealed by Zika virus
440 full-length NS1 structure. *EMBO J* **35**, 2170-2178, doi:10.15252/embj.201695290 (2016).
441 12 Wang, D. *et al.* A Mutation Identified in Neonatal Microcephaly Destabilizes Zika Virus NS1
442 Assembly in Vitro. *Sci Rep* **7**, 42580, doi:10.1038/srep42580 (2017).

13 Muller, D. A. *et al.* Structure of the dengue virus glycoprotein non-structural protein 1 by electron microscopy and single-particle analysis. *J Gen Virol* **93**, 771-779, doi:10.1099/vir.0.039321-0 (2012).
14 Gutsche, I. *et al.* Secreted dengue virus nonstructural protein NS1 is an atypical barrel-shaped high-density lipoprotein. *Proc Natl Acad Sci U S A* **108**, 8003-8008, doi:10.1073/pnas.1017338108 (2011).
15 Scheres, S. H. RELION: implementation of a Bayesian approach to cryo-EM structure determination. *J Struct Biol* **180**, 519-530, doi:10.1016/j.jsb.2012.09.006 (2012).
16 Punjani, A., Rubinstein, J. L., Fleet, D. J. & Brubaker, M. A. cryoSPARC: algorithms for rapid unsupervised cryo-EM structure determination. *Nat Methods* **14**, 290-296, doi:10.1038/nmeth.4169 (2017).
17 Punjani, A., Zhang, H. & Fleet, D. J. Non-uniform refinement: adaptive regularization improves single-particle cryo-EM reconstruction. *Nat Methods* **17**, 1214-1221, doi:10.1038/s41592-020-00990-8 (2020).
18 Pettersen, E. F. *et al.* UCSF Chimera--a visualization system for exploratory research and analysis. *J Comput Chem* **25**, 1605-1612, doi:10.1002/jcc.20084 (2004).
19 Modhiran, N. *et al.* A broadly protective antibody that targets the flavivirus NS1 protein. *Science* **371**, 190-194, doi:10.1126/science.abb9425 (2021).
20 Biering, S. B. *et al.* Structural basis for antibody inhibition of flavivirus NS1-triggered endothelial dysfunction. *Science* **371**, 194-200, doi:10.1126/science.abc0476 (2021).
21 Flamand, M. *et al.* Dengue virus type 1 nonstructural glycoprotein NS1 is secreted from mammalian cells as a soluble hexamer in a glycosylation-dependent fashion. *J Virol* **73**, 6104-6110, doi:10.1128/JVI.73.7.6104-6110.1999 (1999).
22 Syzdykova, L. R. *et al.* Fluorescent tagging the NS1 protein in yellow fever virus: Replication-capable viruses which produce the secretory GFP-NS1 fusion protein. *Virus Res* **294**, 198291, doi:10.1016/j.virusres.2020.198291 (2021).
23 Zheng, S. Q. *et al.* MotionCor2: anisotropic correction of beam-induced motion for improved cryo-electron microscopy. *Nat Methods* **14**, 331-332, doi:10.1038/nmeth.4193 (2017).
24 Tegunov, D. & Cramer, P. Real-time cryo-electron microscopy data preprocessing with Warp. *Nat Methods* **16**, 1146-1152, doi:10.1038/s41592-019-0580-y (2019).
25 Kucukelbir, A., Sigworth, F. J. & Tagare, H. D. Quantifying the local resolution of cryo-EM density maps. *Nat Methods* **11**, 63-65, doi:10.1038/nmeth.2727 (2014).
26 Emsley, P. & Cowtan, K. Coot: model-building tools for molecular graphics. *Acta Crystallogr D Biol Crystallogr* **60**, 2126-2132, doi:10.1107/S0907444904019158 (2004).
27 Adams, P. D. *et al.* PHENIX: a comprehensive Python-based system for macromolecular structure solution. *Acta Crystallogr D Biol Crystallogr* **66**, 213-221, doi:10.1107/S0907444909052925 (2010).
28 Williams, C. J. *et al.* MolProbity: More and better reference data for improved all-atom structure validation. *Protein Sci* **27**, 293-315, doi:10.1002/pro.3330 (2018).

Acknowledgments

We thank Valerie S-Y Chew, Xinni Lim and Qunfei Zhou for help in experiments. This work was supported by Duke-NUS Signature Research Programme funded by the Ministry of Health, Singapore and National Research Foundation Investigatorship award (NRF-NRFI2016-01) awarded to SML. AWKT is supported by a Khoo Postdoctoral Fellowship Award (Duke-NUS-KPFA/2021/0044) from Duke-NUS Medical School and the Estate of Tan Sri Khoo Teck Puat.

Author information

Affiliations

Program in Emerging Infectious Diseases, Duke-National University of Singapore Medical School, Singapore 169857, Singapore.

Bo Shu, Justin S.G. Ooi, Aaron W.K Tan, Thiam-Seng Ng, Guntur Fibriansah, Victor A. Kostyuchenko, Shee-Mei Lok

Centre for Bio-Imaging Sciences, Department of Biological Sciences, National University of Singapore, Singapore 117557, Singapore.

Bo Shu, Aaron W.K Tan, Thiam-Seng Ng, Guntur Fibriansah, Victor A. Kostyuchenko, Shee-Mei Lok

Center for Bioimaging Sciences, National University of Singapore, Singapore, 117557, Singapore.

Jian Shi, Shee-Mei Lok

Medical Sciences Division, University of Oxford, Oxford OX3 9D

Wanwisa Dejnirattisai, Juthathip Mongkolsapaya, Gavin Screaton

Contributions

S.M.L. supervised the project. S.M.L. and B.S. designed research studies; J.S.G.O. produced sNS1. W.D., J.M. and G.S. produced Fab. B.S. and J.S.G.O. conducted experiments. T.S.N., A.W.K.T. and J.S. collected cryo-EM data; S.M.L., B.S., G.F. and V.A.K. analyzed data; S.M.L. and B.S. wrote the manuscript.

Corresponding author

Correspondence to Shee-Mei Lok.

Ethics declarations

Competing interests

The authors declare no competing interests.

Additional information

Extended Data Fig. 1

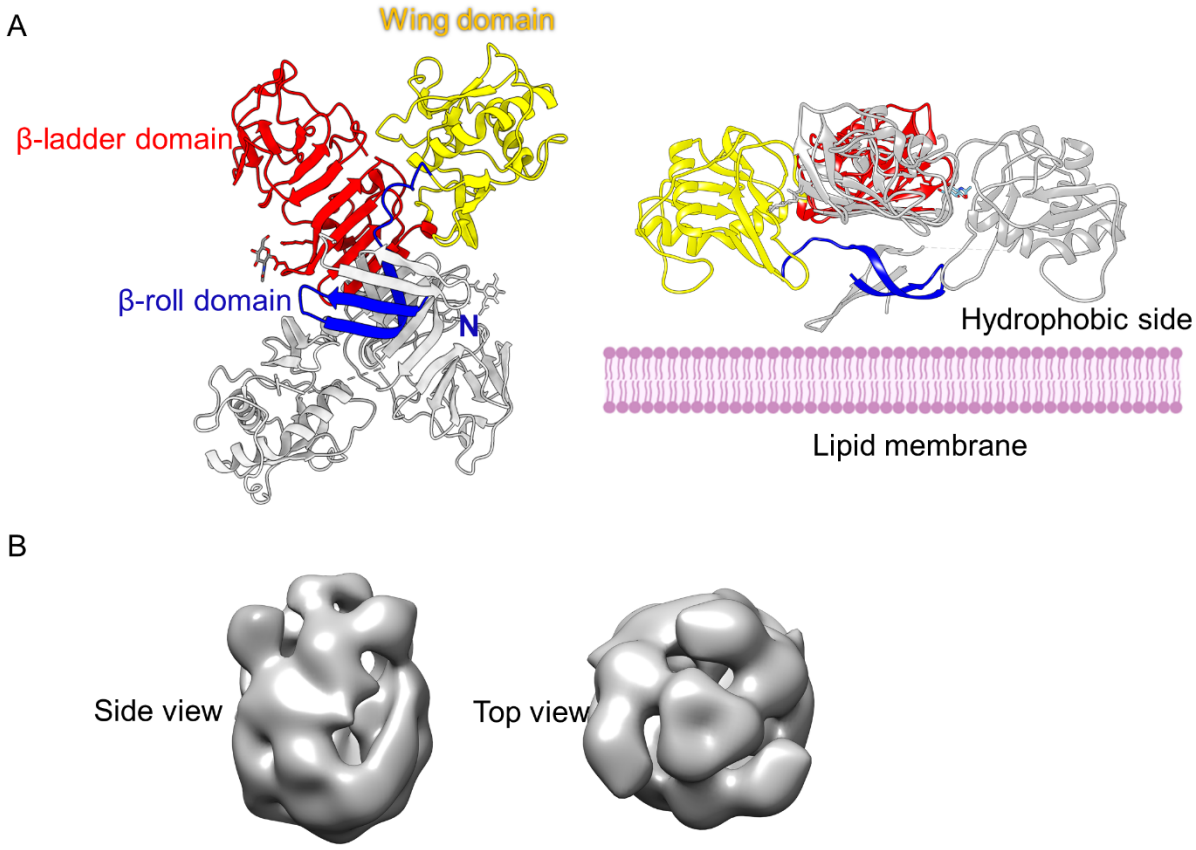

Extended Data Fig. 1 Previously published structures of the dengue NS1. (A) Crystal structure of dengue dimeric iNS1 (PDB:5GS6). Left: top view, looking from the β-roll of the iNS1 dimer. One protomer contains three domains: starting from the N-terminus- β-roll (blue), wing domain (yellow) and the β-ladder (red). It interacts with the other protomer (colored in grey) through extensive hydrogen bonds. Right: side view of the iNS1 dimer. The β-roll is highly hydrophobic and is predicted to interact with the cellular membrane. (B) A previously published low resolution EM reconstruction of the sNS1 (EMDB:2073). This map is reconstructed from negatively stained sNS1 and C3 symmetry was imposed [13].

537

538 **Extended Data Fig. 2**

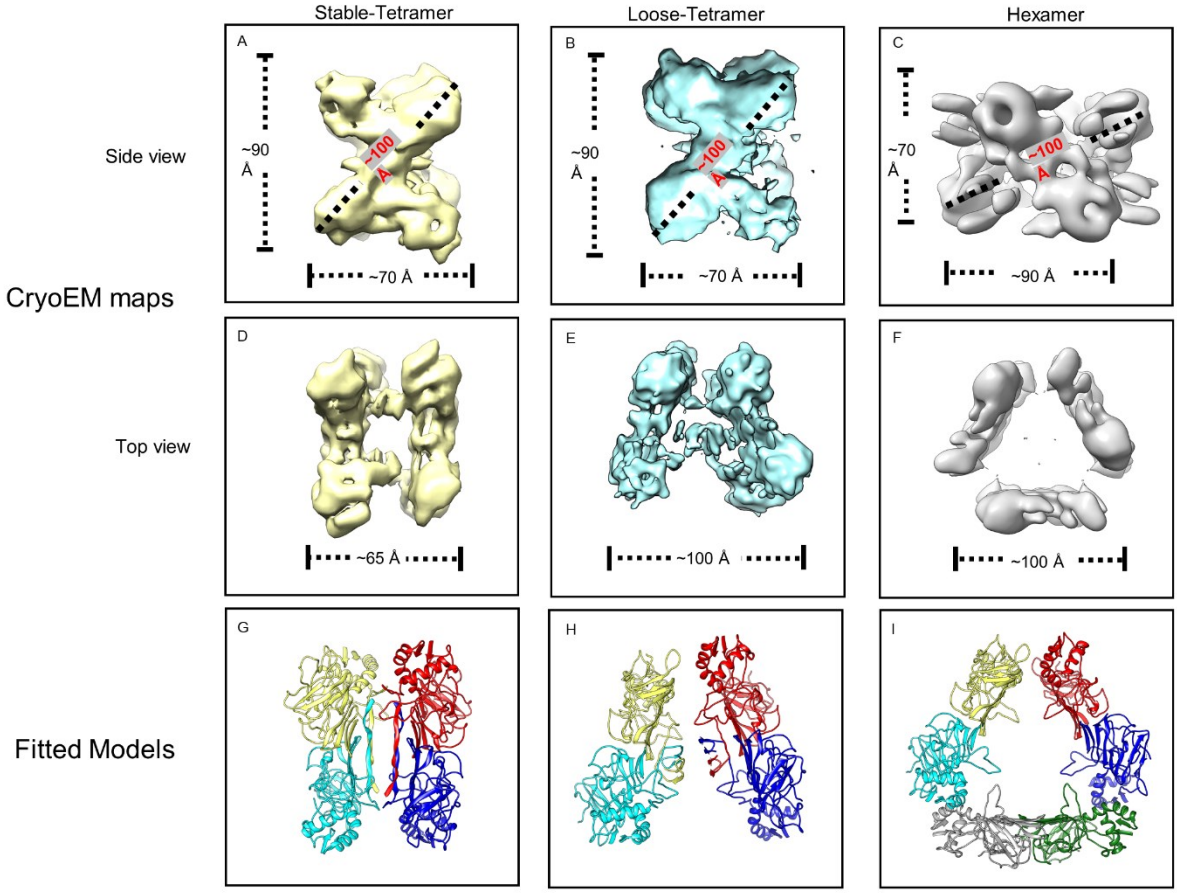

539

540 **Extended Data Fig. 2 The initial sNS1 cryoEM maps after 3D classification using C1**
541 **symmetry.** Dimensions of the stable, loose tetramers and hexamers are shown. Fitted models
542 are shown on the bottom row.

543

544 **Extended Data Fig. 3**

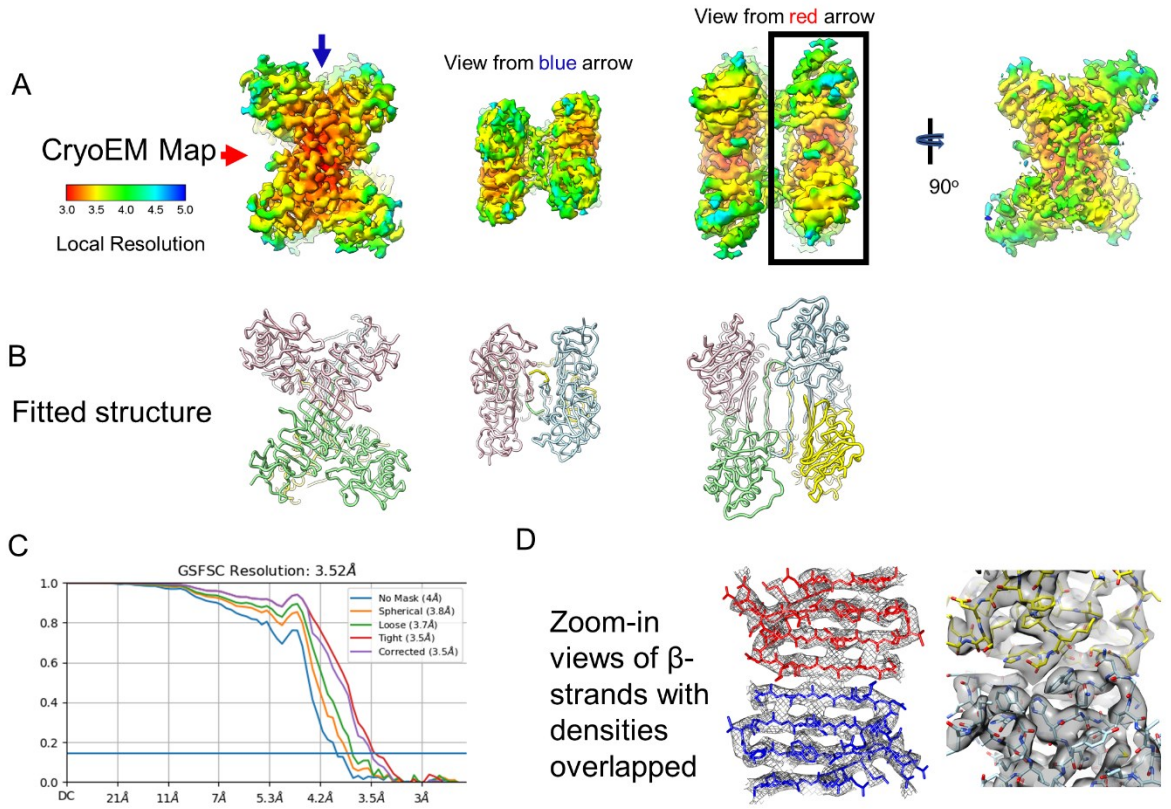

545

546 **Extended Data Fig. 3 The 3.5Å resolution sNS1 stable tetrameric structure.** (A) Different
547 views of the cryoEM map displayed at high contour level. The densities are colored
548 according to their local resolution. (B) The fitted structure show in the same view as the
549 cryoEM map directly above (in (A)). There are two dimers facing each other. One dimer is
550 colored in pink and green, while the other is light blue and yellow. (C) Fourier shell
551 correlation plot showing resolution. (D) Zoom-in views of density map showing the β-strands
552 densities are well resolved (left). Some of the side chains densities (right) can also be
553 observed.

554

555

556

557 **Extended Data Fig. 4**

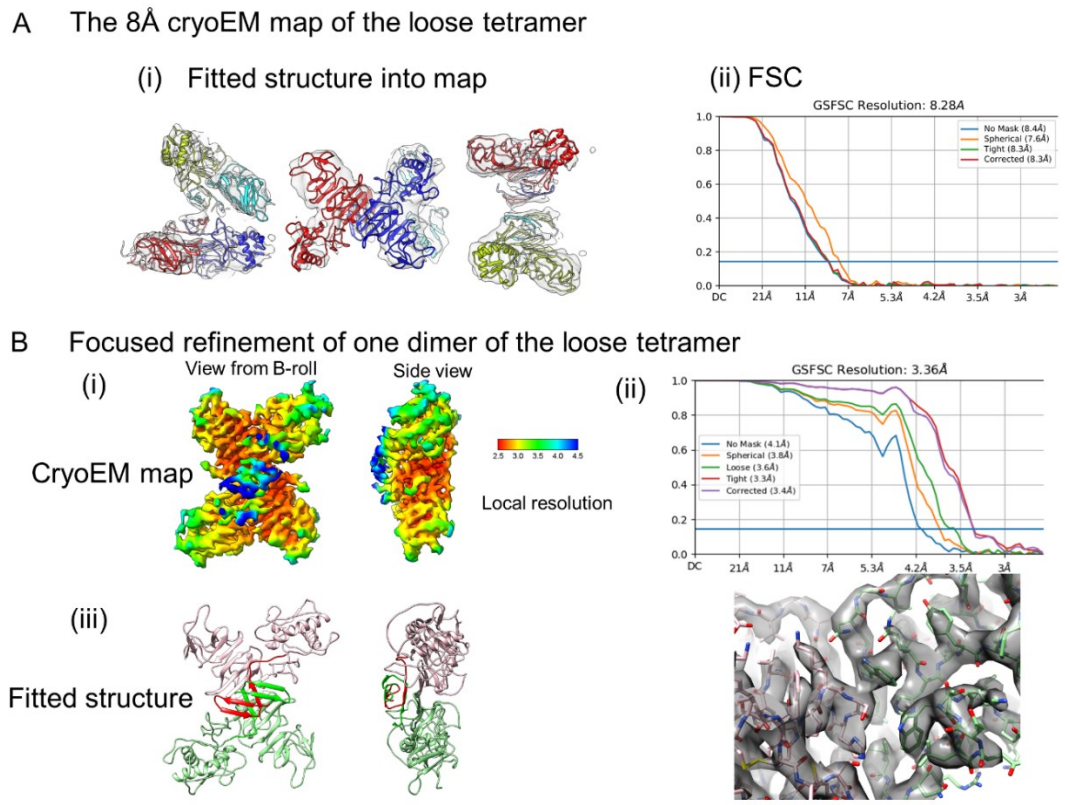

558

559 **Extended Data Fig. 4 CryoEM maps of the sNS1 loose tetramer.** (A) 8Å cryoEM map of the loose
560 tetramer. (i) Different views of the fitted structure of the loose tetramer into the density map
561 (transparent grey). (ii) FSC plot showing resolution. (B) The 3.4Å cryoEM map of one dimer of the
562 loose tetramer after focused refinement. (i) Different views of the cryoEM map. Density is colored
563 according to local resolution. (ii) Up: FSC plot showing resolution of the map: Down: zoom-in view
564 showing that some side chain densities are well resolved. (iii) The fitted structure of one of the dimers
565 (pink and light green) is very similar to that of dengue iNS1. The β-roll in each protomer is colored in
566 a darker shade of the respective protomer's color.

567 **Extended Data Fig. 5**

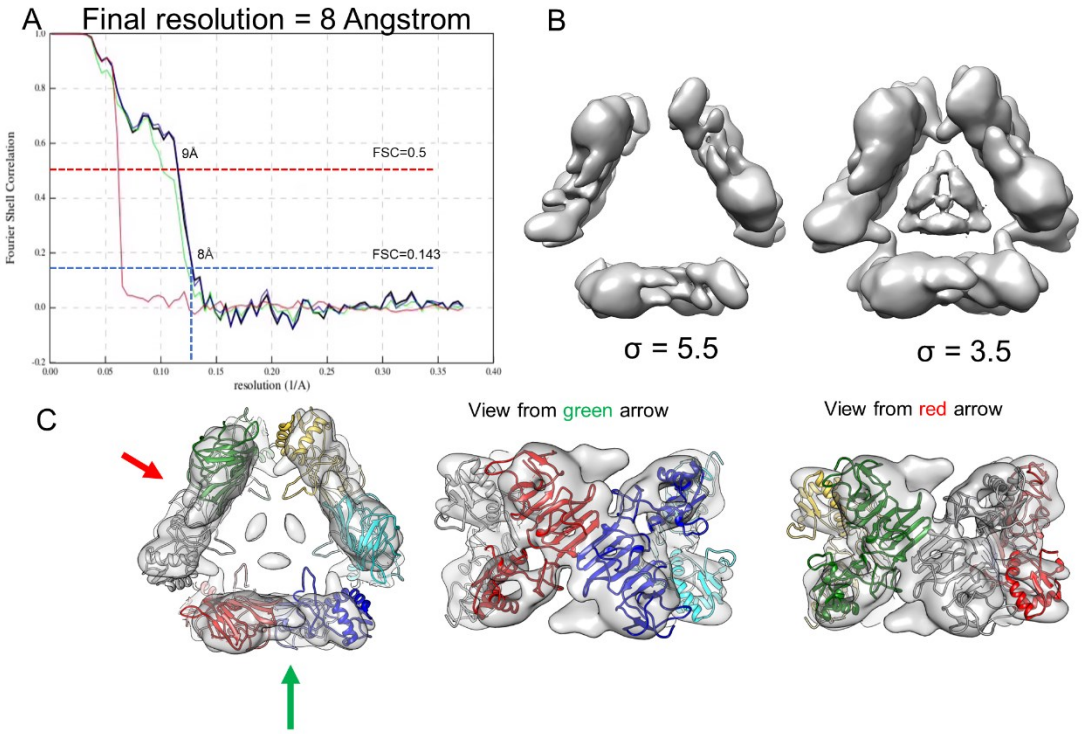

568

569 **Extended Data Fig. 5 The 8Å cryoEM map of the sNS1 hexamer.** (A) FSC plot showing
570 resolution of the map. (B) The hexamer density displayed at different contour levels. At lower
571 contour levels, densities at the interior of the hexamer can be seen. (C) Different views of the
572 fit of the three dimers into the hexamer density map.

573

574 **Extended Data Fig. 6**

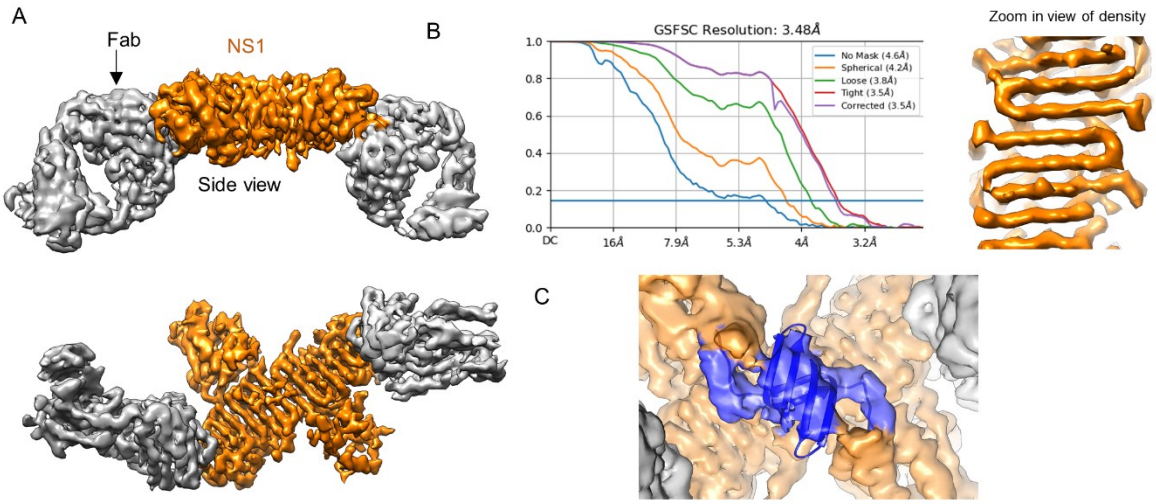

575

576 **Extended Data Fig. 6 3.5Å resolution cryoEM structure of Fab 5E3:sNS1 dimer.** (A)
577 Side and top views of the cryoEM map of the Fab 5E3:sNS1 dimer. NS1 is colored in orange
578 while Fabs in grey. (B) Left: FSC plot showing the resolution of the map. Right: zoom-in
579 view showing well-resolved β-strands. (C) Zoom-in view of the fitted β-roll into its
580 corresponding density.

581

582

583 **Extended Data Fig. 7**

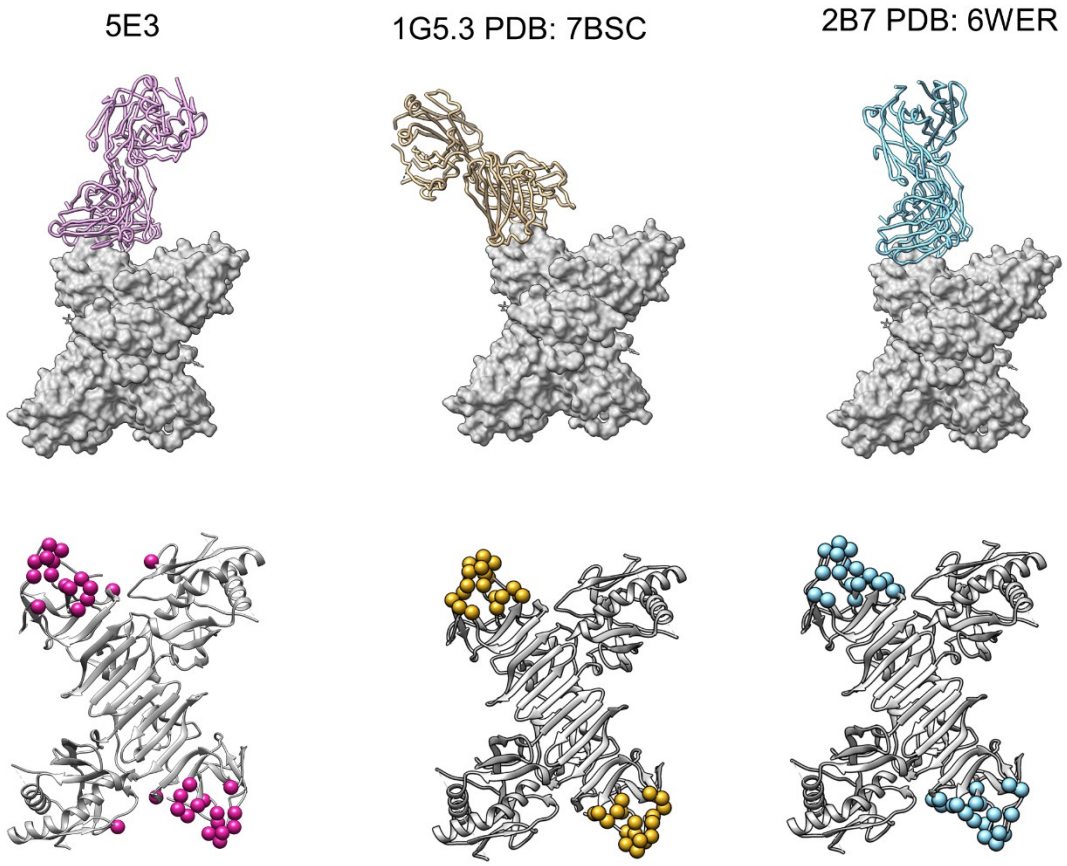

584

585

586 **Extended Data Fig. 7 Comparison of the binding (top panels) and epitope (bottom**
587 **panels) of Fab 5E3 to other previously published Fab:NS1 complexes [19,20].**

588

589

590 **Extended Data Fig. 8**

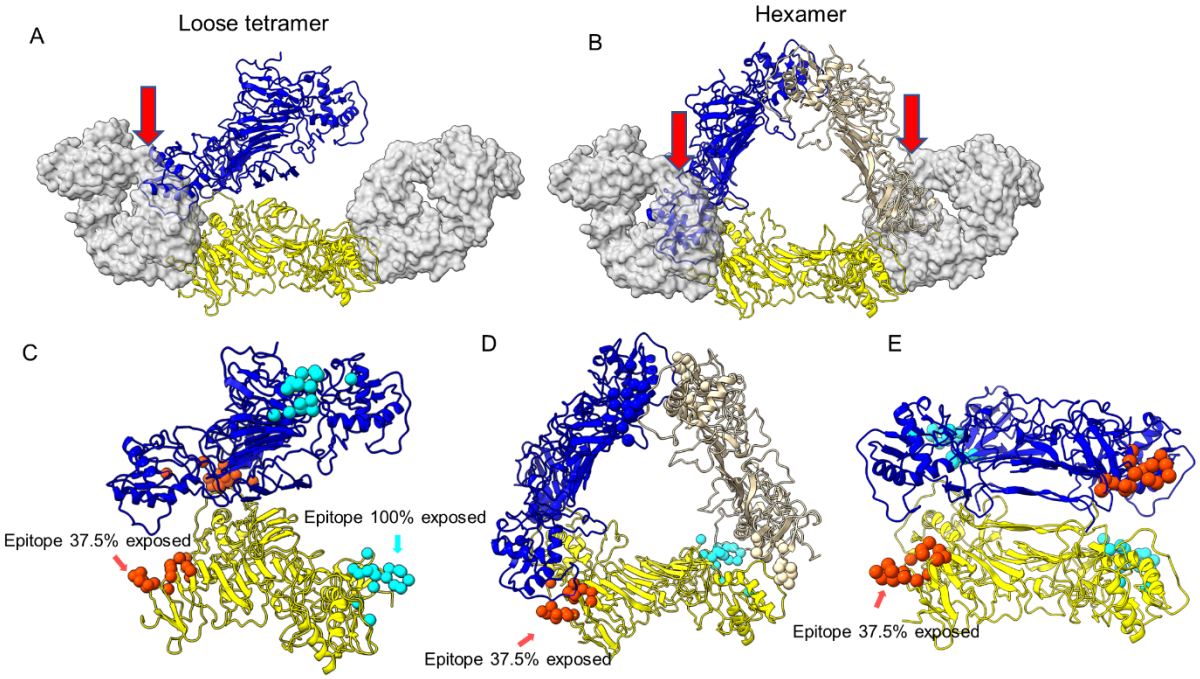

591

592 **Extended Data Fig. 8** Superposition of Fab 5E3:dimer into the (A) loose tetramer and (B)
593 hexamer and the analysis of percentage exposure of epitopes (C-E) in the stable, loose
594 tetramers and hexamers. (A-B) Superposition of Fab 5E3:dimer onto one dimer (yellow) of
595 the loose tetramer and hexamer. Fab is shown as transparent grey surface and clashes with
596 neighboribg NS1 dimer is indicated with red arrows. (C-E) The percentage exposure of
597 epitopes in the oligomers. The two epitopes within one dimer are colored in orange and cyan.
598 (C) In the loose tetramer, 37.5% of the orange epitope is exposed while the cyan epitope is
599 fully exposed (100%). (D) In the hexamer, 37.5% of both the orange and cyan epitopes are
600 exposed. (E) In the stable tetramer, the two epitopes are both 37.5% exposed.

601

602

	Stable Tetramer	Loose Tetramer	Hexamer
Particles	126130	90928	0
Percentage	58%	42%	0 %

Extended Data Table 1 The percentage of particles in different oligomerization states determined after 3D classification of NS1 treated with detergent (0.05% DDM).

NS1	Fab Heavy Chain	Fab Light Chain
138		27(CDR1)
269		94(CDR3)
281	52/53/54/55/56(CDR2)	
299	102/103(CDR3)	
301	33(CDR1)	
302	103(CDR3)	
303	103(CDR3)	
304	32/106(CDR1/CDR3)	
305	31/33/103(CDR1/CDR3)	
306	31(CDR1)	
307	31/53(CDR1/CDR2)	
324	56(CDR2)	
325	57(CDR2)	
326	57/102/100(CDR2/CDR3)	
327	100/102(CDR3)	94(CDR3)
328	100(CDR3)	

Extended Data Table S2 List of hydrogen bonds/electrostatic interactions between Fab 5E3 (heavy and light chains) with the NS1 protein. The interacting CDRs of the Fabs are indicated.